SANDIA REPORT
SAND2026-18248
Printed March 5th, 2026

Sandia National Laboratories

2025 Mykonos Facility Report

Jens Schwarz, Michael Abere, Thomas Awe, Jacob Banasek, Bruno Bauer, Maren Hatch, Nathan Hines, Derek Lamppa, Mike Lowinske, Tyler Mason, Alex Sarracino, and Kevin Yates

Prepared by
Sandia National Laboratories
Albuquerque, New Mexico 87185
Livermore, California 94550

Issued by Sandia National Laboratories, operated for the United States Department of Energy by National Technology & Engineering Solutions of Sandia, LLC.

Printed in the United States of America. This report has been reproduced directly from the best available copy.

Available to DOE and DOE contractors from

U.S. Department of Energy
Office of Scientific and Technical Information
P.O. Box 62
Oak Ridge, TN 37831

Telephone:	(865) 576-8401
Facsimile:	(865) 576-5728
E-Mail:	reports@osti.gov
Online ordering:	http://www.osti.gov/scitech

Available to the public from

U.S. Department of Commerce
National Technical Information Service
5301 Shawnee Road
Alexandria, VA 22312

Telephone:	(800) 553-6847
Facsimile:	(703) 605-6900
E-Mail:	orders@ntis.gov
Online order:	https://classic.ntis.gov/help/order-methods

National Nuclear Security Administration

DEDICATION

In Memoriam Michael G. Mazarakis ⋆ 1937 † 2026

Thanks for giving us the gift of Mykonos

ABSTRACT

This document summarizes the activities at the Mykonos Pulsed Power Facility during the calendar year 2025. Section 1 reports on the yearly shot statistics along with some facility highlights. Section 2 discusses the many improvements we were able to complete this year, thanks to the generous Mykonos Academic Access Programs (MAAP) funding from SSAP and Sandia strategic investments. Section 3 focuses on each individual campaign and their respective results.

ACKNOWLEDGEMENT

Running the Mykonos facility is a tremendous team effort and relies largely on staff that are taking time out from their regular duties in order to perform functions at the Mykonos accelerator.
At the heart of the facility are the experimenters from Sandia and across the US, together with the students that keep this research facility at the forefront of science and innovation while fostering a new generation of bright minds.
A number of our staff and students have volunteered to become Mykonos shot operators, firing the machine, not just for their own campaigns, but also for their fellow researchers.
Furthermore, we have a dedicated team of highly trained technologists that perform daily refurbishment and experiment support, as well as yearly maintenance on top off their regular duties. They take this accelerator apart each year for refurbishment and assemble it back for another year of reliable operation.
Pulsed power science expertise and troubleshooting is provided by senior scientists and highly trained technologists.
Finally, I would like to acknowledge the support of the Advanced Diagnostic (AD) Program who kept this facility vibrant for more than a decade now. Recently, we have been fortunate to get funding for our Mykonos Academic Access Program (MAAP) through Stewardship Science Academic Program (SSAP), Corporate Assessment, and ZNetUS.[1] This funding has allowed us to perform a series of much needed upgrades of diagnostics, infrastructure, and engineered safety systems (see section 2).

- **Experimenters:** Tom Awe, Jacob Banasek, Bruno Bauer, Asher Beck, Ashish Dahal, Maren Hatch, Nathan Hines, Derek Lamppa, Mike Lowinske, Alex Sarracino, Alexander van Balderen, and Kevin Yates
- **Shot Operators:** Karen DeZetter, Maren Hatch, Nathan Hines, Derek Lamppa, Alex Sarracino, and Kevin Yates
- **Facility Upgrades:** Kevin Austin, Jacob Banasek, Bill Bui, Karen DeZetter, Maren Hatch, Ed Holman, Mark Kimmel, Derek Lamppa, Mike Lowinske, Mike Montoya, Robert Obregon, Patrick Rambo, Dan Scoglietti, Lauren Singer, and Shane Speas,
- **Technologists:** *Daily Operation:* Robert Obregon; *Yearly Maintenance:* Eric Breden, Tommy Mulville
- **Pulsed Power Science and Troubleshooting:** Brian Hutsel, Karen DeZetter, Derek Lamppa, and Adam Steiner

[1]This work was supported by the National Nuclear Security Administration through the Support for Academic Programs contract 89233121FNA400377.

This page intentionally left blank.

CONTENTS

This page intentionally left blank.

LIST OF FIGURES

This page intentionally left blank.

LIST OF TABLES

This page intentionally left blank.

ACRONYMS & DEFINITIONS

ABM Applied B-field on Mykonos

ABZ Applied B-field on Z

AD Advanced Diagnostic

AK Anode - Cathode

APD Avalanche Photo-Diode

ASAP Assured Survivability and Agility with Pulsed Power

ASW Audio Square Wave

CY Calendar Year

ED Engineered Defect

EMF Electromagnetic Force

EOS Equation of State

ETI Electrothermal Instability

FWHM Full Width at Half Maximum

ICCD Intensified Charged Coupled Device

ICF Inertial Confinement Fusion

LCM Load Current Multiplier

LDRD Laboratory Directed Research and Development

MAAP Mykonos Academic Access Program

MagLIF Magnetized Liner Inertial Fusion

MHD Magneto Hydro-Dynamic

MITL Magnetically Insulated Transmission Line

MP3 Mykonos Parallel Plate Platform

MRTI Magneto Rayleigh Taylor Instability

OTS Optical Thomson Scattering

PCD Photo-Conducting Diamond

PD Principal Designer

PDV Photon Doppler Velocimetry

PE Principal Experimenter

PIC Particle In Cell

REHEDS Radiation, Electrical, and High Energy Density Science

SHOP-DI Second Harmonic Orthogonal Polarization - Dispersion Interferometer

SI Strategic Investment

SiD Silicon Diode

SSAP Stewardship Science Academic Program

SVS Streaked Visible Spectroscopy

UFP3 Uniform Field Parallel Plate Platform

UXI Ultra-fast X-ray Imager

XRD X-Ray Diode

ZNetUS Z-pinch Network United States

1. SUMMARY OF FACILITY SHOTS AND FUNDING SOURCES

This report briefly summarizes the activities at the Mykonos Pulsed Power Facility during the calendar year 2025. This was the second full calendar year of the "Mykonos Academic Access Program" (MAAP). New funding for MAAP and ZNetUS, as well as strategic investments (SI) from Sandia, allowed for significant upgrades to the facility and its operation which is discussed in section 2.

For calendar year 2025, we performed a total of 219 shots across ten different experimental campaigns (see Fig. 1-1 (a)) that were largely funded through LDRD and the Advanced Diagnostic (AD) Program (see Fig. 1-1 (b)). No ZNetUS campaigns were performed in CY2025 due to the late second ZNetUS user call.

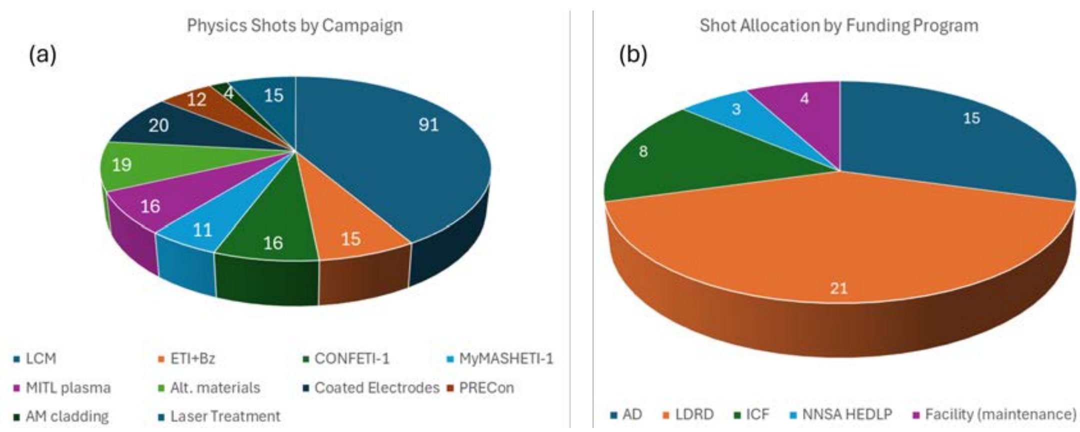

Figure 1-1. (a) Number of physics shots by campaign, and (b) number of shot weeks for respective funding program.

We set three new facility records:

- We performed the largest number of physics/experiment shots in a single day (24)
- We conducted 91 physics shots in just 3.5 weeks
- Produced the highest current at Mykonos to date: 1.6 MA, a 60% increase.

The MAAP is also very proud to report that we supported a total of seven students across six universities in the United States (Cornell, TTU, Rochester/LLE, UNM, UNR, and UW).

For calendar year 2026, we have been awarded three campaigns by ZNetUS for a total of nine weeks in the areas of low density plasma diagnostics (UNM), power flow physics (UNR), and astrophysical plasmas (Caltech).

Detailed listing of funding sources

NNSA Funding

Funding Program	Contract#
SSAP	89233121FNA400377
Corporate Assessment	
HEDLP	DE-NA0004135 and DE-NA0004136

Table 1-1. MAAP funding was provided through SSAP and Corporate Assessment, which in turn allowed for the facility improvements and campaign support reported below.

LDRD

Project#	Title
236981, REHEDS	Optical Thomson Scattering to characterize low-density plasmas on Mykonos
229427, REHEDS	Evolution of the electrothermal instability ...
235699, ASAP	Non-uniform Joule heating and plasma formation ...
229447, ASAP	Laser modification and Coating of MITL surfaces
233048, ASAP	Additively manufactured refractory claddings for MITL surfaces

Table 1-2. List of LDRD projects (Investment Area, and Title) that have funded facility upgrades and shot campaigns.

NNSA program funding

- Sandia supported critical program R&D (liner instability, advanced concepts, power flow physics) on Mykonos through the **ICF** and **Advanced Diagnostics** programs.

Sandia Internal Funding

- Sandia committed significant resources through its' **Strategic Investment (SI)** allocation which funded the OTS beam transport infrastructure.

2. FACILITY IMPROVEMENTS

This year's upgrades were focused on expanding our diagnostic capabilities and the addition of an external B-field capability subsystem.

2.1. Beam transport line for Optical Thomson Scattering Diagnostic

Sandia provided a significant strategic investment in CY25 in order to build a two beam transport infrastructure that connects the Z-Backlighter facility to Mykonos (see Fig. 2-1). This enables the beam transport of the 532 nm Chaco laser [3] beam into the Mykonos target chamber. This system can provide up to 50 J in 10 ns or 5 J in 500 ps, ideal for Optical Thomson Scattering (OTS) and x-ray backlighting, both of which we plan to demonstrate in CY26. A second beam line is reserved for the expansion of future capabilities, namely the addition of ultra-short pulse lasers at 800 nm.

Figure 2-1. (top) Laser beam vacuum transport lines from Z-Backlighter (back wall) to the Mykonos Laser Control Area (left). (right) Beam steering tower. (bottom) Down periscope for beam routing into target chamber and alignment beam injection area and beam diagnostic (bread board).

2.2. 10 T external B-field capability

The Mykonos Accelerator Operations team has designed, integrated, and commissioned an applied magnetic field capability into Mykonos (ABM) that delivers $\approx$ 10 T to a nominal 40 cm^3 load volume in the vacuum load region (see Fig. 2-2). This subsystem [1] enables studies of liner surface plasma formation, instability growth, and magnetized power flow conditions relevant to ICF campaigns on the Z Machine. This capability was used on a two-week campaign for twelve Mykonos shots. The system design leveraged experience gained from designing and operating the Applied Magnetic Field on Z (ABZ) subsystem as utilized on Magnetized Liner Inertial Fusion (MagLIF) Z experiments. Unlike the ABZ single-use coils, the electromagnet assembly can be reused on Mykonos; a single coil assembly has been used for all eighteen 10 T shots to date.

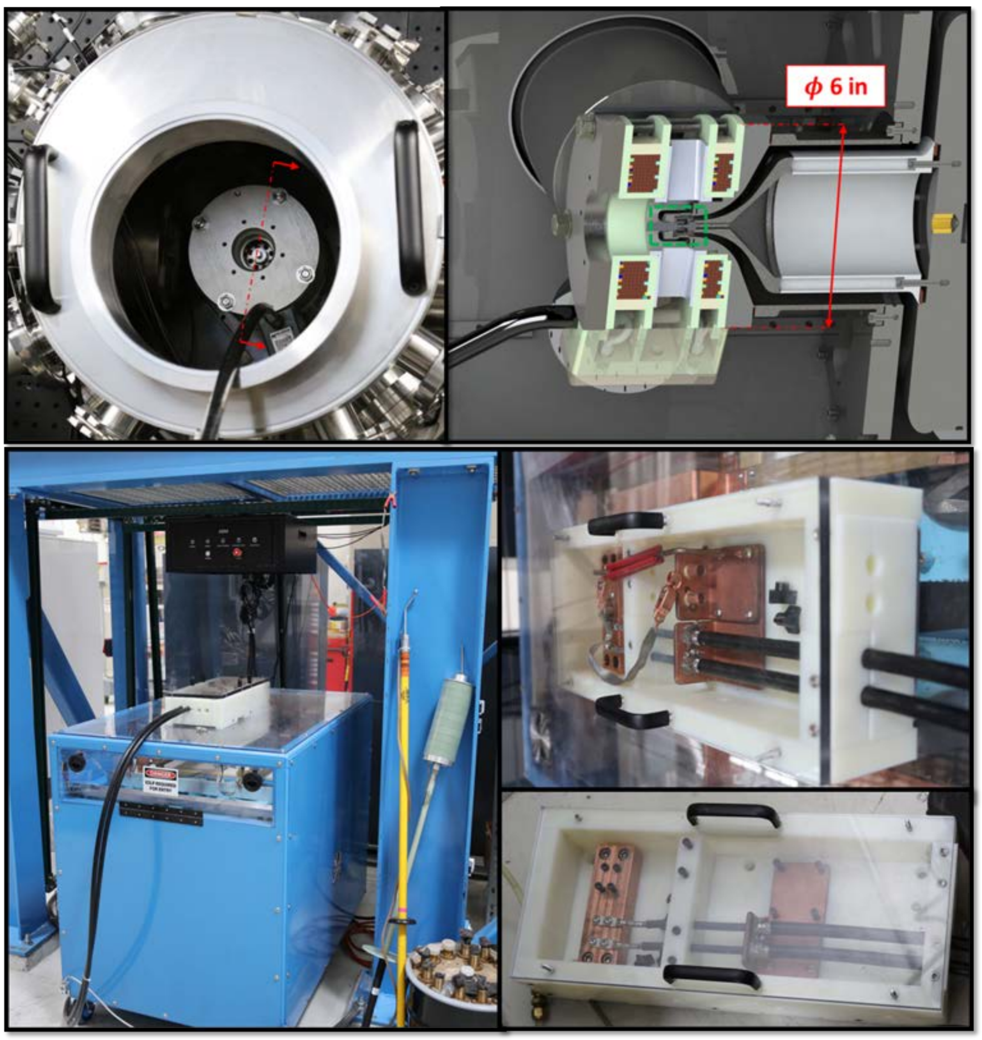

Figure 2-2. (top)The Applied B on Mykonos coil system (left) with intermediate vacuum lid in place. A rendered half-section through the indicated line (right) shows a Helmholtz-like coil pair capable of magnetizing Mykonos targets within the $\approx 40\,\mathrm{cm}^3$ load volume (dotted green box) to ≈ 10 T. (bottom) The ABM system deployed at Mykonos, with debris shielding and hard- and soft-grounding sticks (left). The ABM Junction Box for the two output cables (upper right) mounted atop the ABM bank.

2.3. X-ray backlighting diagnostic

A new point projection radiography capability was commissioned on the Mykonos pulsed power facility in November, 2024. Molybdenum wires were used in an X-pinch configuration on the return path of the $\approx 1\,\text{MA}$, 100 ns current to generate high-quality x-ray radiographs of exploding z-pinch rods. Figure 2-3 shows images of instability structures on the target surface, demonstrating a capability that will provide valuable datasets to compare with simulation and theory. This diagnostic has since been used for other experimental series to evaluate how the electrothermal instability (ETI) is impacted by subsurface inclusions in the target material.

Since November of 2024, the x-pinch radiography capability has been fielded on multiple physics platforms, requiring an upgrade in hardware and diagnostic access. In 2026, we plan to implement several key enhancements: hardware design modifications to accommodate most diagnostic access positions within the chamber, the integration of B-dot probes for monitoring current through the x-pinch, and the coupling of Sandia's Ultra-Fast Digital X-ray Imager (UXI). The UXI [2] is a high speed, multi-frame, time-gated Read Out Integrated Circuit, developed to take two 2 ns X-ray images with high, 25 μm spatial resolution. An x-pinch "cassette" is also under development to facilitate the assembly and loading of the x-pinch.

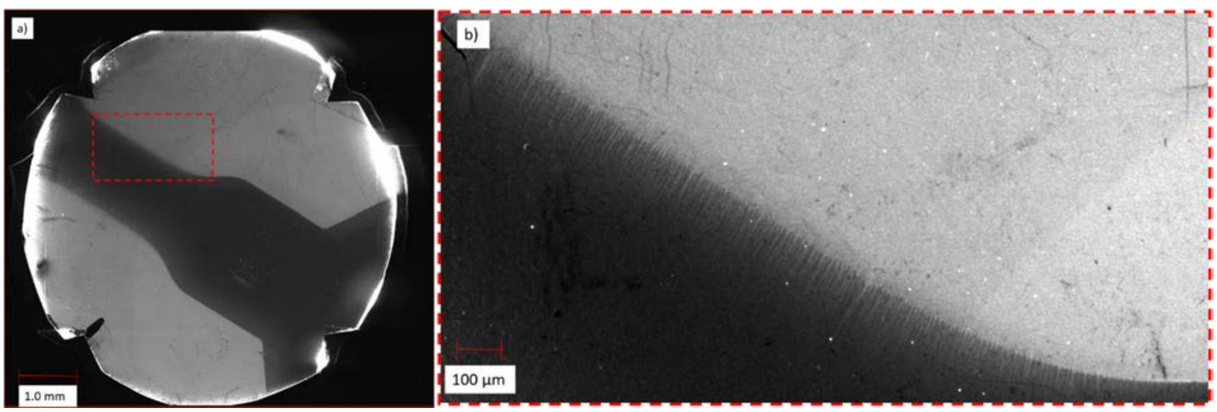

Figure 2-3. (a) X-ray radiograph of the lower two-thirds of an aluminum ETI z-pinch target. The red dashed box indicates the section of the target magnified in figure b). (b) Magnified image of the edge of the same z-pinch target, with instability structures visible on the surface of the target.

2.4. Dedicated SVS diagnostic for Mykonos

Figure 2-4 shows the dedicated streaked visible spectroscopy (SVS) system that has recently been deployed on Mykonos. The SVS system had previously been shared with the Z facility and hence would be unavailable when conflicts with the Z schedule arose. The streak camera is an Optronis with a wide range of sweep speeds, starting at a few ns full sweep and going up from there. The spectrometer is a 2/3-meter McPherson which can have spectral bandwidths and resolutions ranging from 300 nm with a 3.6 nm FWHM on a 50 l/mm grating down to 7 nm with a 0.08 nm FWHM with a 2400 l/mm grating. These features make it suitable for a wide variety of applications on Mykonos.

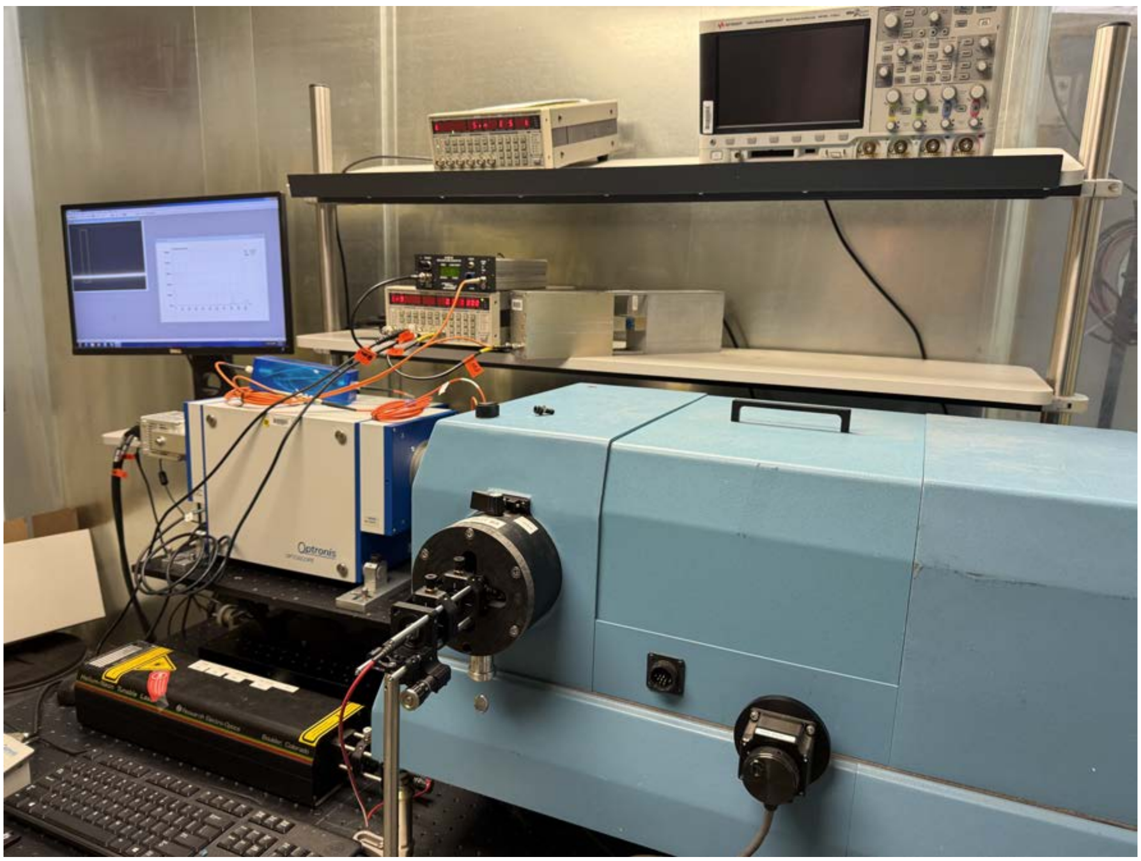

Figure 2-4. SVS system inside the Mykonos clean room. One can see the spectrometer (blue, right) being attached to the streak camera (white, left), with the calibration laser (black) below.

2.5. Commissioning of Compact Load Current Multiplier (LCM)

Figure 2-5 shows a Compact Load Current Multiplier (LCM) that was designed and tested in a series of experiments on Mykonos in October and November 2025. LCMs increase driver-to-load energy transfer efficiency for low-inductance targets, where $L_{Load} \ll L_{excluder}$, using the principle of an impedance transformer. The heart of LCM functionality is a flux excluder which, in principle, is a conductive cavity surrounding the load-current path. Lenz's law stipulates that a directionally-opposing current will form on the exterior of this conductor. These two current paths can be combined by connecting the excluder in parallel with the load, thus causing current multiplication. The compact LCM developed is a removable assembly that consists of an anode cap, the flux excluder, and an AK bridge. Four Bdots mounted to the anode cap, evenly spaced at 90° intervals, monitor current in the load region and serve as the diagnostic instrumentation for the experiments. The LCM module can be inserted between the anode and cathode inside the chamber and the AK bridge – a solid stainless steel rod – spans this gap.

Both conventional machining and additive manufacturing were used to produce the inner flux excluders – the former for the primary test pieces, and the latter to serve as proof-of-concept for the use of 3D printed parts on Mykonos. The outer flux excluder is a stainless steel cylindrical shell, which contains 4 tabs extending up to the anode cap to serve as the convolute posts. All outer excluders were conventionally machined. Both inner and outer excluders were expected to be damaged by testing, so multiple copies of each were made, but it was discovered that each routinely survived >10 shots. Experimental results indicated that peak load current multiplication of >1.5 was achieved.

Figure 2-5. The as-built Compact LCM Module, with the four B-dot probes on top.

This page intentionally left blank.

3. MYKONOS CAMPAIGNS IN 2025

3.1. LCM Demonstration on the Mykonos driver

Primary Goals: The campaign aimed to demonstrate load current multiplication on a small scale as proof-of-concept for future application on Z. A secondary goal was testing the viability of additive manufacturing for experimental hardware fielded on Mykonos.
Results: Tests were conducted across a sweep of charge voltages from 50-85 kV using conventionally machined flux excluders possessing variable gap sizes. Tests were similarly run on additively manufactured flux excluders – both rough and post-machined – with variable gap sizes.
Experimental results demonstrated that load current multiplication of >1.5 was achieved across the range of charge voltages and gap sizes. 3D printed flux excluders with slight post-machining maintained integrity under full-load conditions and provided near-equivalent performance with that of conventionally machined excluders.
Multiple new facility records were set, including peak current (1.6 MA at an 85 kV charge voltage), number of shots conducted in a single day (24), and total shots conducted on a campaign interrogating a physics load (91).
Publications: Papers will be submitted in CY26 to Review of Scientific Instruments for the hardware design and Physics of Plasmas for in-depth theory and results.
Researchers: *PE:* Maren Hatch, Mike Lowinske *Key Collaborators:* Chris Jennings (PD, simulation), Derek Lamppa (simulation, analysis), Nathan Brown, Nicki Bennett.
Funding Program: ICF
Number of weeks and number of shots: 3.5 weeks, 91 physics shots
Diagnostics: B-dot current probes

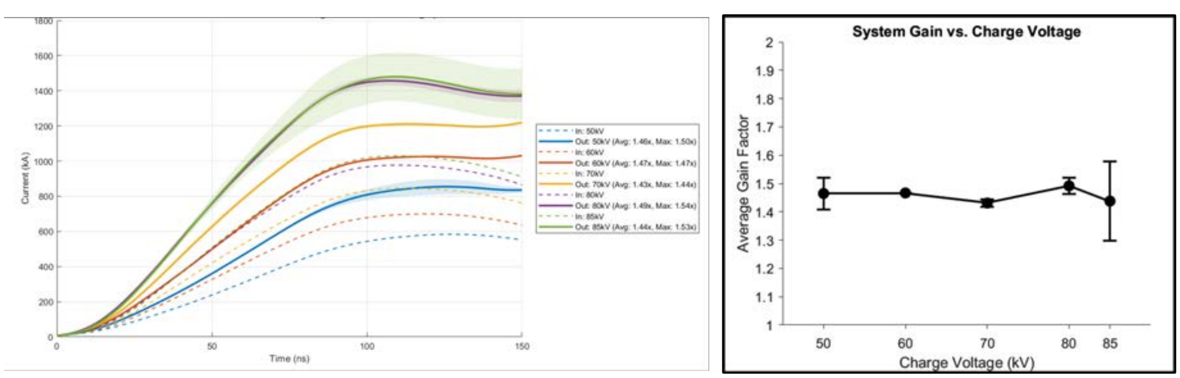

Figure 3-1. Plot of Mykonos load current for various charge voltages. The dashed lines are baselines traces (without the LCM) and the solid lines are the amplified current measurements.

3.2. ETI+B_Z: Static Axial Field

Primary Goals: Electrothermal instability (ETI) evolution on a z-pinch rod is expected to be modified when the magnetic field changes from purely azimuthal (B_Θ) to helical ($B_\Theta + B_Z$). Specific emission patterns are expected to re-orient along the field lines. Experimental data were gathered to test this hypothesis using "engineered defect (ED)" targets while using a newly commissioned Helmholtz coil pair to drive a slowly rising (≈ 2 ms) 10 T axial magnetic field, B_Z, throughout the experimental hardware (see Fig. 3-2). Prior to firing Mykonos, the B_Z field is fully diffused and "static" within the z pinch rod.

Results: When a quasi-hemispherical ED is machined into the surface of a thick z-pinch rod, current density is diverted around the ED, introducing symmetric azimuthal current density, j_Θ. In the presence of a fully diffused (static) axial field, once the surface of the rod begins to expand, the motional EMF term ($v_r \times B_Z$) in Ohm's Law drives an additional j_Θ EMF term, which results in asymmetry in the current flow around the ED, driving overheating which amplifies with time, and eventually leads to a helically oriented overheating pattern. Simulations using accessible experimental parameters suggested that the expected helically oriented patterns would be quite subtle. Therefore, a new and deeper ED type was milled into the rod's surface to accentuate the asymmetric heating. Unfortunately, the new machining technique resulted in undesirable surface defects, including burrs, which altered ED emissions. As a result, the ETI physics objectives of the experiment were not met. However, a new static axial field capability was commissioned on Mykonos. The system delivered the requested 10 T axial field on all 11 downline ETI experiments.

Publications: An article (lead author, Lamppa) is planned for Rev. Sci. Instr., which will detail the design and performance of the newly commissioned Applied B on Mykonos (ABM)
Researchers: *PE:* Tom Awe; *Theory/Sim:* Edmund Yu, Gabe Shipley; *ABM Development Team:* Derek Lamppa, Ed Holman, F. Sanchez; *Key Collaborators:* Kevin Yates, Kurt Tomlinson (GA)
Funding Program: LDRD# 229427 (REHEDS)
Number of weeks and number of shots: 2 weeks, 15 Physics shots, 11 shots with the static field
Diagnostics: ICCDs, B-dots (including downstream of the target); ABM electrical diagnostics

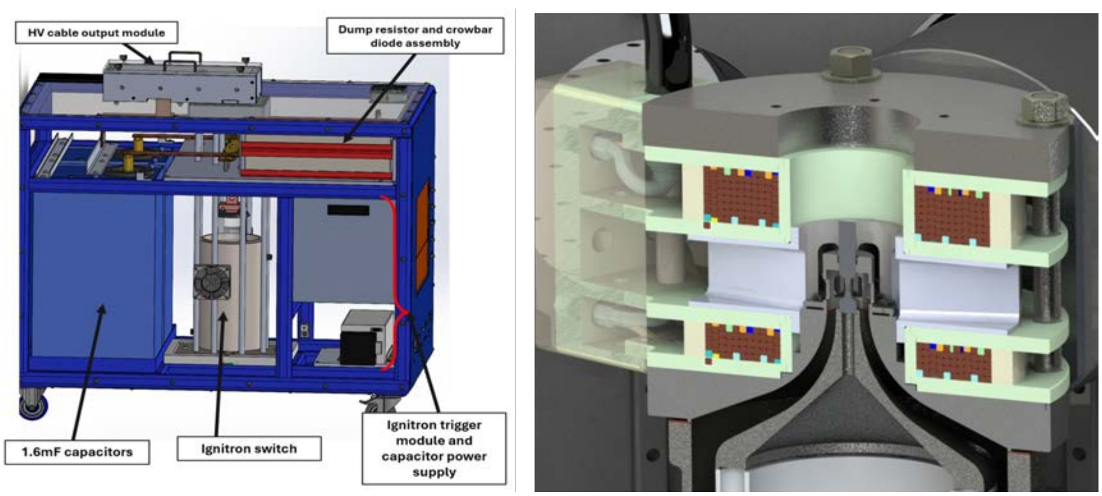

Figure 3-2. (Left) ABM pulsed power system and (right) in chamber Helmholz coils.

3.3. CONFETI-1: Coatings on flat face ETI targets

Primary Goals: The objective of CONFET-I on Mykonos was to develop methods to assess the impact of embedded inclusions on ETI growth. This campaign interrogated the deposition and behavior of ion-beam deposited 6N aluminum coatings on aluminum targets of varying composition, introducing a novel target design for future ETI platforms. The second part of the CONFETI campaign will draw on results from CONFETI-1 but will include buried microspheres underneath the aluminum coating.

Results: The findings of this first campaign showed that ultra-pure coatings largely tamped visible ETI surface emissions. The 6N aluminum coatings behaved as expected when applied on both ultra-pure 6N aluminum as well as on aluminum 6061, which contains many more voids and inclusions. Surface emissions were not visible through a 20 μm thick coating of the pure 6N Al, but emissions were more visible from beneath a 5 μm coating (see Fig. 3-3).

Publications: This dataset will contribute in part to a graduate student dissertation and peer-reviewed articles.

Researchers: *PE:* Maren Hatch, Asher Beck; *Key Collaborators:* Bruno Bauer, Ashish Dahal, Tom Awe

University collaborations/Students: Asher Beck (University of Washington), Prof. Bruno Bauer, Ashish Dahal (University of Nevada, Reno).

Funding Program: LDRD# 235699, MAAP

Number of weeks and number of shots: 3 weeks, 16 physics shots

Diagnostics: ICCDs, B-dots, PDV, photodiode radiometry, x-pinch radiography, PCD/SiDs

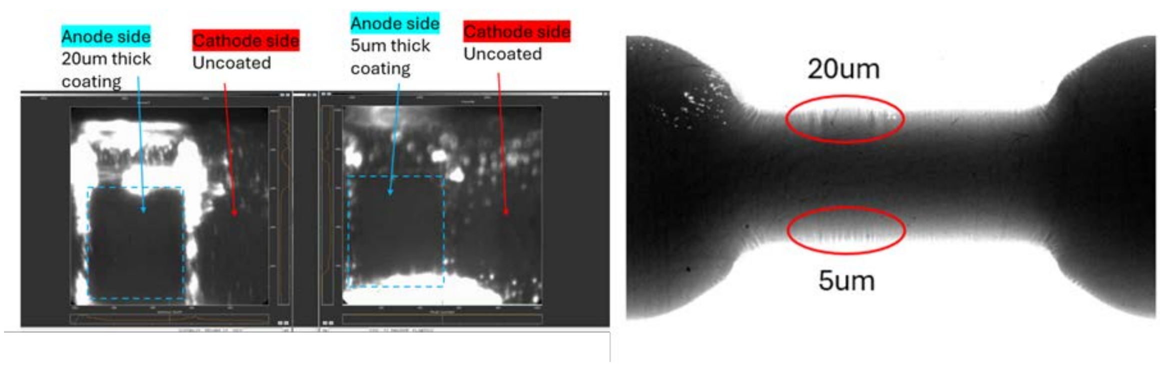

Figure 3-3. (left) Intensified CCD camera image of a coated (20 μm thick) and an uncoated region of a 6061-aluminum barbell. Visible emissions are largely suppressed under such a coating. (middle) Intensified CCD camera image of a coated (5 μm thick) and an uncoated region of a 6061-aluminum barbell. Visible emissions are slightly suppressed under such a coating, when compared to uncoated region. (right) X-ray radiograph of the same target type. The 20 μm thick coating can be seen on the top of the target, while the 5 μm coating is on the bottom of the image. Instabilities persist under the coatings, despite the suppression of the visible emissions.

3.4. MyMASHETI-1: Mykonos MITL plasma impact on load surface hydrodynamics and ETI

Primary Goals: We set out to observe the impact of plasma from a perturbed magnetically insulated transmission line (MITL) on the expansion and electrothermal instability (ETI) of a pulsed-power-driven aluminum rod. This would open a new dimension in ETI experiments, beyond observing the effects of current density, material properties, and surface features.

Results: Figure 3-4 shows that transmission-line contact quality made a strong impact on downstream load brightness and ETI growth. ICCDs recorded strong azimuthal variations of load brightness and ETI that followed imposed azimuthal cathode-button contact variations. The observations are consistent with charged particles from intentionally sharp edges at specific azimuthal locations in the otherwise axisymmetric MITL, flowing to the load surface via the $E \times B$ drift at constant azimuthal angle, locally altering surface heating. This result helps develop Mykonos as a platform for improving predictive capability for MITL plasma effects on loads and diagnostics.

Publications: This dataset will contribute in part to a graduate student dissertation and peer-reviewed articles.
Researchers: *PE:* Prof. Bruno Bauer (UNR); *Key Collaborators:* Maren Hatch, Mark Gilmore, Tom Awe, and Kevin Yates
University collaborations/Students: Ashish Dahal (University of Nevada, Reno), Asher Beck (University of Washington), Alexander van Balderen (University of New Mexico)
Funding Program:DOE-NNSA HEDLP Awards DE-NA0004135 and DE-NA0004136
Number of weeks and number of shots: 3 weeks, 11 physics shots
Diagnostics: ICCDs, B-dots, PDV, photodiode radiometry, x-pinch radiography, PCD/SiDs

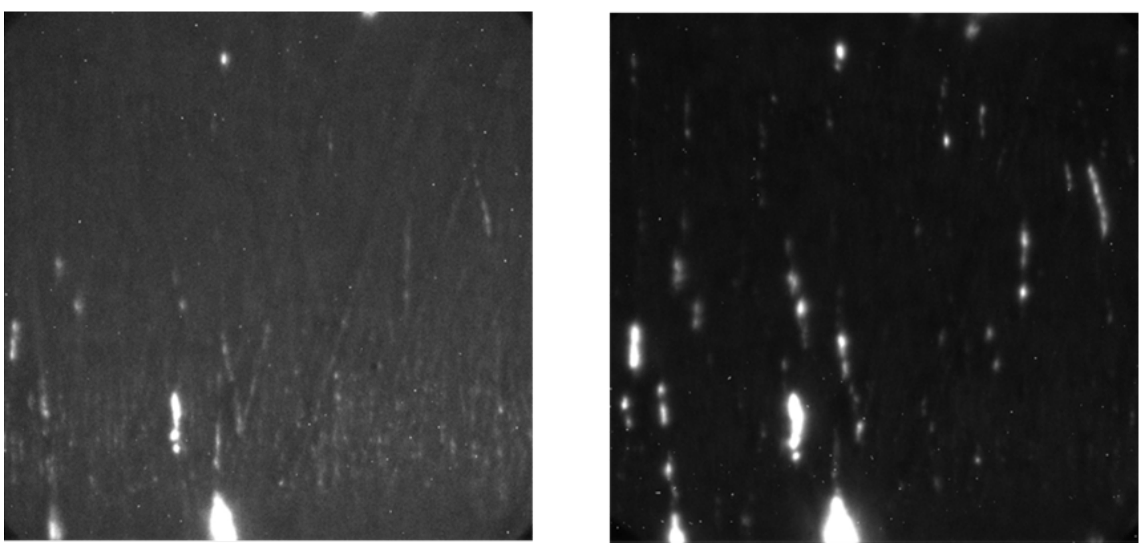

Figure 3-4. Increased Al-1100 rod surface brightness and ETI due to an upstream (out of view) mm-protruding Cu foil at the cathode-to-barbell contact. The axial current is horizontal in the 3 ns ICCD images, while azimuthally correlated ETI is vertical. The Cu foil was just below the rest of the contact for azimuthal angles corresponding to the (dimmer) top half of the images, but just above for the (brighter) bottom half.

3.5. MITL Plasma Formation and Transport Studies

Primary Goals: The 2025 campaign's primary goal was to begin fielding the Second-Harmonic Orthogonally Polarized Dispersion Interferometer (SHOP-DI) diagnostic at a probing location near the Mykonos Parallel Plate Platform (MP3) hardware's anode surface (see Fig. 3-5). This anode surface plasma formation data would then be compared against the 2024 experimentally obtained cathode surface plasma formation data, as well as against the recently conducted 2D and 3D CHICAGO Particle-In-Cell (PIC) simulations of the MP3 hardware's plasma behavior. A secondary goal was the implementation of new SHOP-DI inner vacuum chamber lens relay mounting and alignment hardware.

Results: The campaign was largely a success. Anode surface plasma data for 4 different MP3 hardware geometries were collected. Analysis of this data with comparisons against previous cathode surface data and recent CHICAGO PIC simulations are underway. Implementation of the new SHOP-DI inner vacuum chamber lens relay mounting hardware and alignment hardware were successful. Problems arose after the first 16 shots, where the SHOP-DI output polarization state began fluctuating between the pre-shot calibration sweep and the downline current pulse, effectively voiding the calibration sweep and preventing post-shot plasma areal density calculations. Efforts are ongoing to mitigate this issue for future campaigns.

Publications: Presented at PPC/ICOPS 2025. Planned Rev. Sci. Instr./Phys. Rev. STAB sub.
Researchers: *PE:* Nathan Hines
Funding Program: Advanced Diagnostics (AD)
Number of weeks and number of shots: 5 weeks, 16 physics shots
Diagnostics: SHOP-DI, APDs, B-dots, V-dots

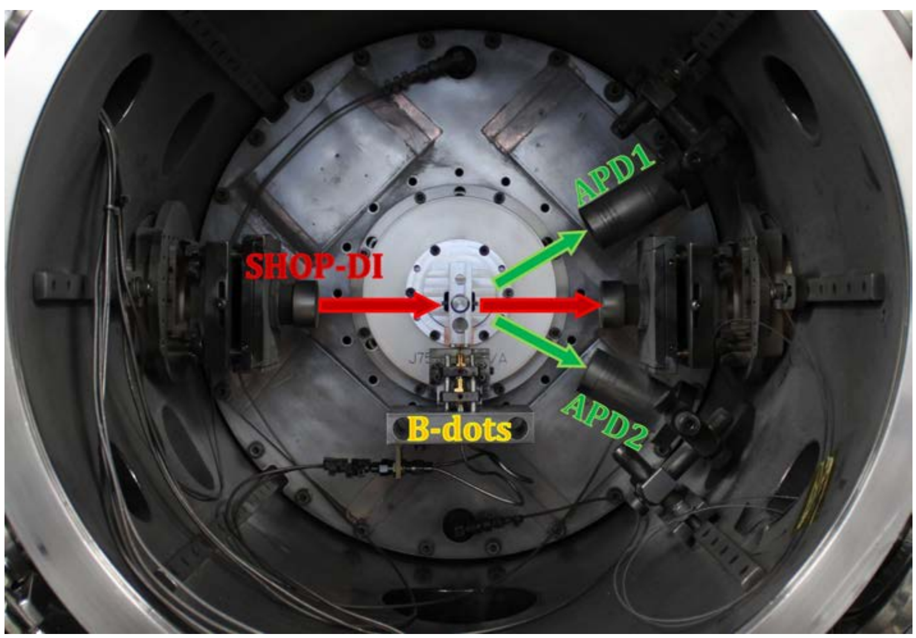

Figure 3-5. SHOP-DI left-to-right probing beam (red), electrode plasma self-emission collection from the anode APD1 and cathode APD2 (green), and parallel plate and load region B-dot probes (orange).

3.6. Study of alternate materials for ICF implosions on Z

Primary Goals: The ETI in metals creates azimuthal perturbations due to $d\eta/dT > 0$, which can act as a possible seed for MRTI. The ability to accurately model these processes is limited by EOS uncertainties and the lack of experimental data. The goal of these experiments is to study alternative materials as possible candidates for reducing early ETI and late time MRTI. Experiments on Mykonos utilized PDV, pyrometry, and iCCD imaging to capture time-resolved surface velocity, temperature, and early time ETI. The metals fielded are titanium (high resistivity) and nickel (high $d\eta/dT$ at room temperature) with both coated (35 μm of dielectric) and uncoated surfaces.

Results: Figure 3-6 shows significant variations in surface heating for nickel and titanium wires. Uncoated titanium melts and explodes many nanoseconds earlier than uncoated nickel and expands with greater radial velocity. Titanium also forms plasma $\approx$ 50 ns earlier than nickel. Interestingly, nickel shows an extended period of heating of 55 ns (295-350 ns) prior to plasma formation compared to the 10 ns (285-295 ns) observed in titanium. Coated nickel and titanium have a similar early emission profile, but quickly diverge at $\approx$ 330 ns, with titanium increasing in self-emission intensity. Gated self-emission imaging captures the early development of non-uniform heating in the form of ETI. Bands of self-emission perpendicular to current flow (indicative of ETI) were not observed on titanium wires. Images of the coated wires were captured and indicate little to no strata; however, more analysis is needed to interpret this data. Results from this campaign are preliminary with significant data analysis needed; however, this data set should help us understand possible paths for utilizing alternative metals or composite materials in our ICF platforms.

Publications: Work will be presented at ICOPS 2026 and PRE, expected late CY26.
Researchers: *PE:* Kevin Yates; *Key Collaborators:* Adam Harvey-Thompson, Tom Awe, Luke Stanek, Edmund Yu, Christopher Jennings, Matthew Weis, Maren Hatch
Funding Program: ICF
Number of weeks and number of shots: 4 weeks, 19 shots
Diagnostics: ICCDs, Bdots, PDV, Pyrometry, x-pinch radiography

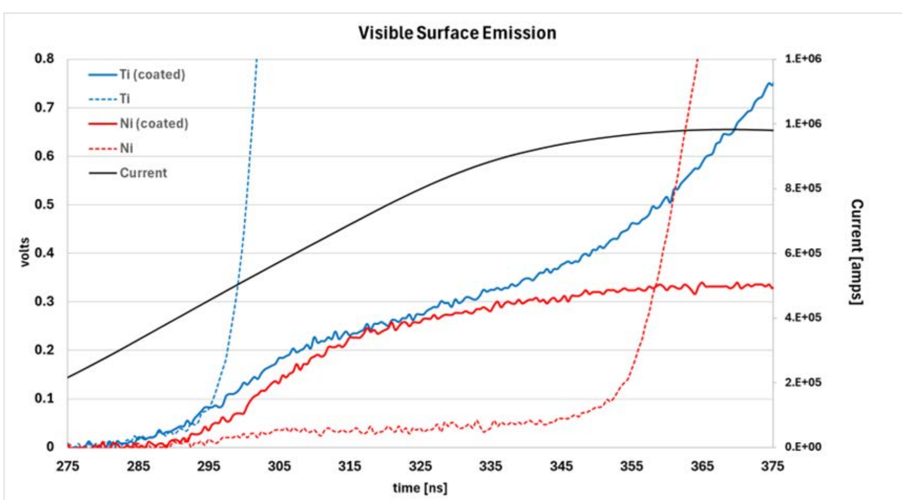

Figure 3-6. Visible emission is captured with time resolved diodes. Variations in heating is oberved between titanium and nickel for both coated and uncoated surfaces.

3.7. Current Loss Mitigation Coatings

Primary Goals: Current loss on Z is primarily attributed to the early thermal desorption of contaminants from electrode materials before their melting occurs. Ex-situ processes aimed at reducing the density or delaying the desorption of these contaminants offer a viable approach to mitigating parasitic current loss in the Z inner MITL and post-hole convolute. In this campaign, three distinct coatings were evaluated for their effectiveness: (1) bi-metallic coating, which consists of a manganese layer atop a copper layer, directing the current sub-surface and reducing the heating rate; (2) silicon carbide (SiC) coating, which serves as a diffusive barrier that inhibits hydrogen from penetrating the gap; and (3) molybdenum (Mo) coating, characterized by a high melting and vaporization temperature and a lower hydrogen concentration compared to stainless steel.

Results: Overall, the coatings appeared to initiate plasma generation later in the pulse and exhibited a lower self-emission intensity, suggesting that plasma density is generally reduced for the coated electrodes compared to the controls. Figure 3-7 (left) illustrates the time elapsed after the start of current at which the self-emission intensity of each sample reaches 50% of the saturation intensity of the detector, categorized by gap spacing. Both the molybdenum and bi-metallic coatings delayed the onset of plasma self-emission by approximately 10 ns, while the SiC coating delayed it by as much as 40 ns. Figure 3-7 (right) presents the mean pixel intensity from the iCCD cameras alongside the corresponding measured AK gap spacing for controls, bi-metallic, and SiC-coated electrodes. The bi-metallic coatings exhibited a plasma self-emission reduction of 40-80% compared to controls with similar gap spacing, whereas the SiC coatings demonstrated a reduction exceeding 90%. Manufacturing issues made the Mo results unreliable, so they were not included. These findings indicate that the application of coatings can significantly impact plasma formation physics. Among the coatings tested, silicon carbide coatings emerged as clear front-runners, demonstrating substantial improvements relative to the controls and other coatings. The bi-metallic performed admirably, and still remains a candidate for adoption on Z.

Publications: Work was presented at IFSA 2025 & planned publication.
Researchers: *PE:* Alex Sarracino, *Key Collaborators:* Tylan Watkins, Steven Larson
University collaborations/Students: Cameron Chavez (Cornell), Alexander van Balderen (UNM)
Funding Program: LDRD# 229447 (ASAP)
Number of weeks/shots: : 5 weeks, 10 Controls, 6 Mn/Cu Bi-Metallic, 2 SiC, 2 Moly
Diagnostics: ICCDs, B-dots, Shadowgraphy, Three Decade Avalanche Photodiodes (APDs), SVS

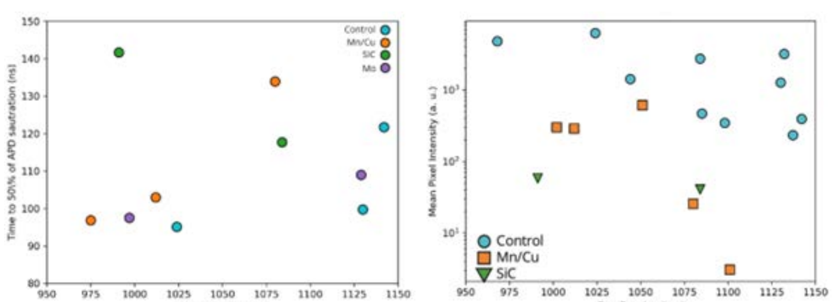

Figure 3-7. (Left) Time elapsed between start of current and turn on of self-emission. (Right) Average plasma self-emission intensity of iCCD images.

3.8. PRECon – In-situ cleaning

Primary Goals: This campaign aimed to field in-situ plasma cleaning on a larger parallel plate cross-sectional geometry and evaluate effectiveness on a lower current density platform. The MiniXRD diagnostic was also fielded for the first time to assess bulk electrode and surface plasma temperatures.

Results: The Mykonos Parallel Plate Platform (MP3) provides direct diagnostic access to scaled electrodes that achieve the same magnetic flux density and ohmic heating rates of the Z inner MITL within several centimeters of the Z center axis. This platform was primarily designed as a testbed for demonstrating whether in-situ and ex-situ electrode conditioning techniques can affect the formation and evolution of electrode plasma. In-situ plasma cleaning has been demonstrated to be effective at delaying plasma formation and reducing overall plasma number density, though the process had been fielded most often on the smallest hardware sets that recreate conditions closest to the Z target. This campaign uses larger cross section anodes and cathodes that move the equivalent Z inner MITL further out to the convolute. This series also included the MiniXRD power flow diagnostic as a ridealong. A MiniXRD is a biased copper electrode that collects photoelectrons created by x-rays exceeding 5 eV. A time-resolved effective blackbody temperature of the emitting surface, whether it be bulk electrode or dense surface plasma, can be estimated based on the recorded voltage. Spatial resolution along the electrode can be achieved by introducing a pin-hole aperture at the end of the MiniXRD drift tube to limit the collection to a few mm diameter spot.

Twelve shots were taken in total during this campaign using the 2.5 mm × 1.75 mm load hardware with the wide (2 mm) anode configuration, with AK gaps ranging from 0.84 – 0.98 mm. SVS and APDs were also included in this test campaign to diagnose plasma formation, temperature, and atomic constituency. Six shots were performed without a plasma cleaning process, and six used an audio square wave (ASW) discharge for about an hour prior to downline. Shots with plasma cleaning were divided into two categories; those with MiniXRDs and those without. Those with MiniXRDs (4 of 6) observed little change on electrode plasma evolution. Those without (2 of 6) dramatically reduced the observed plasma, with the larger AK gap spacing shot producing no anode plasma at peak current as detected by the ICCD. A post-series review discovered that the MiniXRDs did not incorporate an effective pump out aperture. During plasma discharges, the drift tubes were filled with process gas, which could not evacuate during the few minutes between plasma extinguishing and downline. The tubes were pumped out through the drift tube pinhole, directing argon oxygen at the test MITLs. This gas load caused those shots to not differ from the control experiments. The MiniXRDs did observe x-ray fluence consistent with plasma temperatures exceeding those predicted by MHD simulation.

Publications: This dataset will contribute to two Physics of Plasmas paper and one dissertation.
Researchers: *PE:* Derek Lamppa, Jacob Banasek, and Alex Sarracino
University collaborations/Students: UNM, Tyler Watson, (TTU)
Funding Program: Advanced Diagnostics (AD)
Number of weeks/shots: : 3 weeks, 12 shots
Diagnostics: and Subsystems ICCDs, SVS, MiniXRDs, APDs, Si photodiodes, Bdots (including downstream of the target), plasma cleaning subsystem

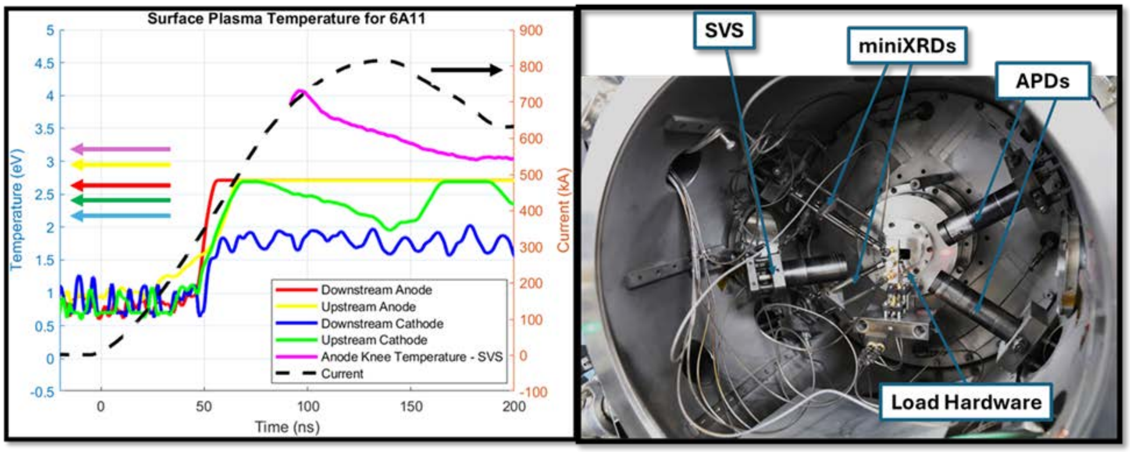

Figure 3-8. MiniXRD traces (left) overlaying current data. The MiniXRD requires light from a plasma exceeding a few eV to generate signals above noise. Signals equivalent to > 2 eV blackbody were observed early in the pulse; such temperatures do not occur in the MHD simulation of the electrode material. The experimental geometry is shown (right) with MiniXRDS, APDs, and SVS lines of sight directed at the 2.5 mm $\times$ 1.75 mm Mykonos parallel plate platform load hardware.

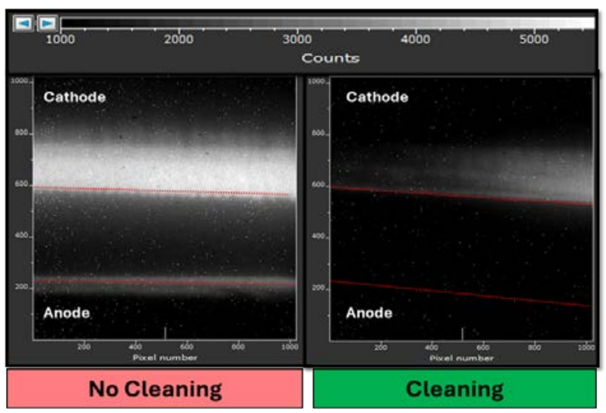

Figure 3-9. ICCD images taken without (left) and with (right) an in-situ plasma glow discharge. Both images were taken near 130ns, which is roughly peak current for Mykonos. The AK gap is 0.97 mm for both these shots. The plasma treatment eliminated the anode electrode plasma at least to the sensitivity to the ICCD, and significantly reduced the intensity of emission for the cathode. These observations are consistent with the plasma process removing surface inventory, lowering the number density of the electrode plasmas.

3.9. Additively manufactured current loss mitigation claddings

Primary Goals: Current loss on Z is largely attributed to the early thermal desorption of analyte species from electrode materials before their melting occurs. Ex-situ processes aimed at reducing the density or delaying the desorption of species such as hydrogen offer a viable approach to mitigating parasitic current loss in the Z inner MITL and post-hole convolute. In this campaign, a new high entropy alloy composed of CoCrFeMoW constituents was tested on Mykonos, as temperature-programmed desorption experiments indicated that it is almost completely hydrogen insoluble. Furthermore, this additively manufactured cladding material is expected to exhibit a refractory-like melting temperature, minimal grain boundaries, and low but metallic electrical conductivity—properties that are all beneficial for MITL cladding.

Results: An artifact of the additive printing process is unfused powder that prevented smooth surfaces on the claddings in the left hand image of Fig. 3-10. The composite nature of the target alloy and unfused powder complicate the assessment of the cladding's effectiveness. The ICCD images captured at a gap spacing of within 10 μm for a control sample (shot 3) and a clad cathode (shot 4) with an unclad anode are also presented in the right of Fig. 3-10. These images show that the unfused powder present in the system possibly contributes to the formation of large nucleation sites for plasma. Notably, away from the most significant manufacturing flaws, the ICCD data indicates approximately 70% intensity at early times. However, at later times, there is increased variability in the intensity observed in the cladding, ranging from 20% to 80% on the cathode. APDs on the cathode also showed $\approx$ 50 ns delay in rise time. It is important to note that the conclusions drawn from these observations are limited. Only a single cathode was sufficiently flat to align properly and not have the weld fail during the experiment. At best, the results suggest that the material does not negatively impact self-emission.

Researchers: *PE:* Michael Abere, Lauren Singer, Alex Sarracino
Funding Program: LDRD# 233048 (ASAP)
Number of weeks/shots: : 1 week, 3 controls, 1 cladding cathode
Diagnostics: and Subsystems ICCDs and APDs

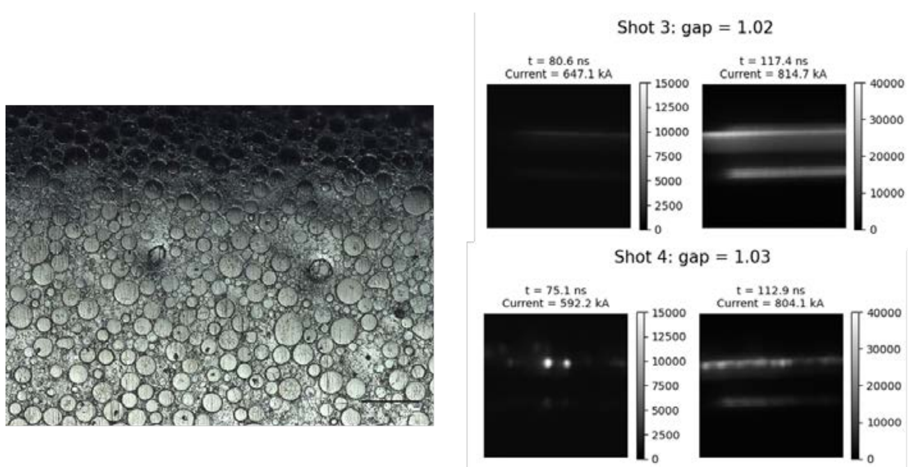

Figure 3-10. (left) Morphology of additively manufactured cladding (right) Shot 3 (Control) and Shot 4 (Cladding on cathode only) at a comparable gap spacing.

3.10. Mitigating current losses due to bulk desorption through laser-stimulated grain growth

Primary Goals: Losses in the inner magnetically insulated lines (MITLs) of the Z machine are thought to be primarily caused by the desorption of surface contaminants containing hydrogen. In this shot series, we sought to probe the role of hydrogen originating from within the bulk material stainless steel. In particular, we were interested in determining if losses could be reduced by manipulating the grain boundaries, which are known to facilitate faster diffusion than through a crystal lattice. The uniform field parallel plate platform (UFP3) was employed, where the electrodes underwent a laser stimulated grain growth procedure.

Results: The laser treatment was shown to grow the crystal grains by a factor of two. Despite challenges in controlling the AK gap spacing, ICCD images showed a slight reduction in plasma formation between control hardware and laser-treated hardware for most comparisons of similar gap spacing, particularly early in time. Moreover, SVS showed a delay in plasma formation and a reduction in luminescence regardless of AK gap spacing.

Researchers: *PE:* Alex Sarracino, Michael Abere
University collaborations/Students: Tyler Mason (University of Rochester, LLE), Cameron Chavez (Cornell)
Funding Program: LDRD#229447 (ASAP)
Number of weeks/shots: : 2 weeks, 15 shots (8 control; 7 treated)
Diagnostics: and Subsystems ICCDs, B-dots, Three Decade Avalanche Photodiodes (APDs), Streaked Visible Spectroscopy (SVS).

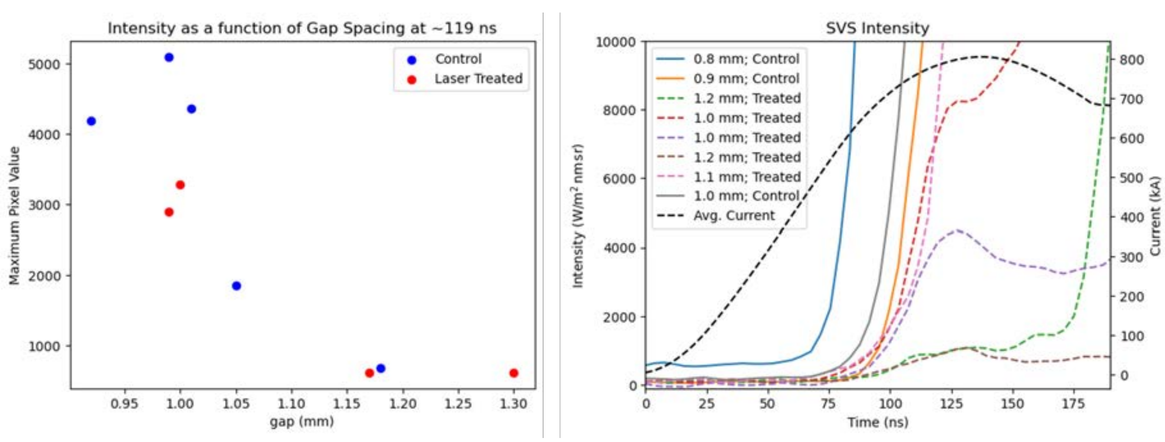

Figure 3-11. (left) The average intensity of ICCD pixels as a function of gap spacing, taken 119 ns into the current pulse. (right) The intensity measured by streaked visible spectroscopy as a function of time. Solid lines show control hardware, while dashed lines show treated hardware.

This page intentionally left blank.

REFERENCES

[1] Thomas James Awe, Edmund Po-ning Yu, Gabriel S Shipley, Derek C Lamppa, Kurt Tomlinson, Edward George Holman, Kevin Colligan Yates, Maren Whiting Hatch, Fernando M Sanchez, and Deanna M Jaramillo. Evolution of the electrothermal instability from thick rod z pinches subject to dynamically and statically applied axial magnetic field. Report, Sandia National Laboratories (SNL-NM), Albuquerque, NM (United States), 2025.

[2] J. L. Porter, Q. Looker, and L. Claus. Hybrid CMOS detectors for high-speed x-ray imaging. *Review of Scientific Instruments*, 94(6), 2023.

[3] P. Rambo, J. Schwarz, M. Schollmeier, M. Geissel, I. Smith, M. Kimmel, C. Speas, J. Shores, D. Armstrong, J. Bellum, E. Field, D. Kletecka, and J. Porter. Sandia's Z-backlighter laser facility. volume 10014, page 100140Z–100140Z–16. 10.1117/12.2245271.

DISTRIBUTION

Email—Internal

Name	Org.	Sandia Email Address
Greg Rochau	1600	garocha@sandia.gov
Michael Cuneo	1650	mecuneo@sandia.gov
Technical Library	1911	sanddocs@sandia.gov

Email—External

Name	Company Email Address	Company Name
Kirk Keilholtz	kirk.keilholtz@nnsa.doe.gov	NNSA
Michael Sheehy	michael.sheehy@nnsa.doe.gov	NNSA
Samantha Calkins	samantha.calkins@nnsa.doe.gov	NNSA
Sarah Nelson	sarah.nelson@nnsa.doe.gov	NNSA
Hanah Joudi	hanah.joudi@nnsa.doe.gov	NNSA
Terri Stone	terri.stone@nnsa.doe.gov	NNSA

This page intentionally left blank.

Sandia National Laboratories